Taylor & Francis
Taylor & Francis Group

Philosophical Magazine Letters

ISSN: 0950-0839 (Print) 1362-3036 (Online) Journal homepage: https://www.tandfonline.com/loi/tphl20

Pinning of grain boundary migration by a coherent particle

Nan Wang, Youhai Wen & Long-Qing Chen

To cite this article: Nan Wang, Youhai Wen & Long-Qing Chen (2014) Pinning of grain boundary migration by a coherent particle, Philosophical Magazine Letters, 94:12, 794-802, DOI: 10.1080/09500839.2014.978408

To link to this article: https://doi.org/10.1080/09500839.2014.978408

Philosophical Magazine Letters, 2014
Vol. 94, No. 12, 794–802, http://dx.doi.org/10.1080/09500839.2014.978408

Pinning of grain boundary migration by a coherent particle

Nan Wang[a]*, Youhai Wen[b] and Long-Qing Chen[a]

[a]*Department of Materials Science and Engineering, Pennsylvania State University, University Park, PA 16802, USA;* [b]*National Energy Technology Laboratory, Albany, OR 97321, USA*

(*Received 8 October 2013; accepted 15 October 2014*)

We studied single-particle pinning of grain boundary (GB) migration during grain growth. A phase-field model was formulated to simulate the pinning by a coherent particle and validated quantitatively by comparison with analytical prediction. A study of GB migration velocity using this model revealed that second-phase coherent particles have a previously unknown restraining effect over the whole of the GB-particle interaction range, which is qualitatively different from the interaction between GB and incoherent particles.

Keywords: grain boundary pinning; coherent precipitate; phase-field; grain growth

Second-phase particles are often employed to inhibit grain growth and stabilize fine-grain structures in polycrystalline materials. The first theoretical attempt to quantify the interaction between a second-phase particle and a grain boundary (GB) was made by Zener [1], and several subsequent works were developed later based on Zener's theory [2–5]. Advances in computational methods for microstructure evolution has made it possible to model the grain growth kinetics and the pinning of second-phase particles using, for example, the Monte-Carlo (MC) method [6–12], the front-tracking finite-element method (FEM) [13–17] and the phase-field (PF) method [18–27]. Among those different computational approaches, the PF method, with its advantage in resolving complex interface motions, has been widely applied in studies of GB motion and microstructure evolution [28,29].

As explained in Zener's theory, the pinning force applied to a moving GB from an incoherent spherical particle is $2\pi r_0\gamma \sin\theta\cos\theta$ [3] where γ is the grain boundary energy, r_0 is the particle radius and the angle θ is defined as that between the GB line and the direction of GB motion at the junction. The maximum pinning force is then $F_z = \pi r_0\gamma$, which is given at $\theta = \pi/4$. Extensions of this theory to non-spherical particle shapes had been developed. For a spheroidal particle with equatorial radius a and pole axis b, the maximum pinning force is $2a\pi\gamma/(1+\varepsilon)$ with aspect ratio $\varepsilon = b/a$ [3]. It has been known that coherently formed second-phase particles exert larger pinning force against a moving GB. As the GB is approaching the pinning particle, part of the originally coherent particle-grain interface joins the GB and loses its coherency. The maximum pinning force from coherent spherical particle, with incoherent interface energy γ_1, coherent interface energy γ_2 and grain boundary energy γ_3, is given by

*Corresponding author. Email: nxw13@psu.edu

$$F_z = \gamma_3 \pi r_0 (1 + \cos\beta), \tag{1}$$

where the joining angle β is defined as that between the GB line and the particle surface tangent. From Young's condition, this is given by $\cos\beta = (\gamma_1 - \gamma_2)/\gamma_3$ [2]. For a generalized ellipsoidal coherent particle, Li et al. [4] carried out a comprehensive numerical study for the pinning force at arbitrary particle orientation, since a general analytical treatment is hard. However, for some cases, deriving an analytical expression for the pinning force from an ellipsoidal coherent particle can be quite straightforward. Here, we start our work by developing a pinning force expression for a coherent prolate spheroidal particle in an axi-symmetric configuration.

A particle in cylindrical coordinates with a grain boundary moving along the z direction is shown in Figure 1. The spheroid surface is $z^2/b^2 + r^2/a^2 = 1$, which can be rewritten as $S = r - a\sqrt{1 - z^2/b^2} = 0$, using $\hat{n} = \nabla S/|\nabla S|$. The local surface orientation is

$$\cos\alpha = \frac{az}{\sqrt{a^2z^2 + b^4 - b^2z^2}} = \frac{\sqrt{a^2 - r^2}}{\sqrt{\varepsilon^2 r^2 - r^2 + a^2}}. \tag{2}$$

The second equality is reached by replacing z with r using the spheroid surface equation. At the GB-particle contact line, using Young's condition $\cos\beta = (\gamma_1 - \gamma_2)/\gamma_3$, the pinning force is simply

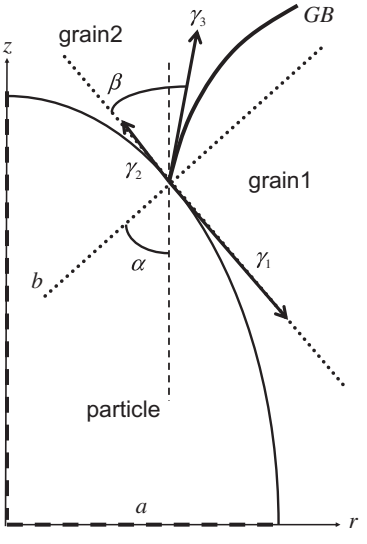

Figure 1. The second-phase particle surface is connected with a GB. Surface energies are labelled as γ_1 for the incoherent interface, γ_2 for the coherent interface and γ_3 for the GB. Two prolate axes are labelled as a and b. β is the angle between the particle surface tangent and the GB line, α is the angle between the z axis and the surface normal.

$$F_z = 2\pi r\gamma_3 \cos[\alpha - (\pi/2 - \beta)]. \tag{3}$$

With the relation between r and α in Equation (2), by eliminating r ,we have

$$F_z = 2\pi\gamma_3 a \frac{\sin\alpha\cos[\alpha - (\pi/2 - \beta)]}{\sqrt{\cos^2\alpha(\varepsilon^2 - 1) + 1}}. \tag{4}$$

For the case of an incoherent particle ($\beta = \pi/2$), taking the derivative of this expression recovers the maximum pinning force for an incoherent prolate spheroid obtained in previous work [3]. For $\varepsilon = 1$, it recovers the formula for coherent spherical particle in Equation (1). The maximum pinning force can be easily evaluated from this expression by plotting F_z as a function of the surface orientation angle α. Although derived in a special configuration, Equation (4) offers a simple way to understand the combined effect of coherency and particle shape.

To simulate particle pinning in grain growth, we follow the PF approach developed by Fan et al. [18] and Moelans et al. [19]. As demonstrated in the work of Harun et al., all three current approaches, the PF method, the front-tracking finite element and the Monte Carlo Potts model, correctly captured the physics of pinning and gave very similar results [12]. The pinning effect of spheroidal particles was studied using the PF model by Vanherpe et al., who found a stronger pinning effect with a higher particle aspect ratio [23]. In the MC study of Kad et al., the effect of particle shape on the grain size was also observed [9]. In a recent work by Chang et al. [25], the single-particle pinning force was quantitatively evaluated using the PF method. By comparing with theoretical predictions, the numerically calculated pinning forces from incoherent spherical and ellipsoidal particle were shown to be accurately reproduced in the PF model. However, this model cannot be applied to study the pinning of coherent particles, since the change of particle-grain interface from coherent to incoherent is not included in the formulation. Here, we present a PF model which incorporates the change of surface energy as the interface switches from coherent to incoherent and validates the model by quantitatively reproducing the coherent particle pinning force proposed in Ashby's work [2].

Based on Chang's work [25], a phase-field model with three order parameters is constructed. The first two order parameters η_1 and η_2 are associated with two grains to model the simplest grain growth (one is growing, the other is shrinking). The third parameter η_3 is used for the pinning particle. The phase-field free energy functional is then [30]

$$F = \int \left[f_0(\eta_1, \eta_2, \eta_3) + \frac{1}{2}\sum_{i=1}^{2} \xi_i K(\nabla\eta_i)^2 + \Delta T h(\eta_1, \eta_2, \eta_3) \right] dv, \tag{5}$$

where the gradient energy coefficient is a product of numerical parameter ξ_i and dimensional constant K, and

$$f_0 = \Delta f \left[\alpha \sum_{i=1}^{2} \left(-\frac{\eta_i^2}{2} + \frac{\eta_i^4}{4} \right) + \sum_{i=1}^{3}\sum_{j<i} \epsilon_{ij}\eta_i^2\eta_j^2 + b\prod_{i=1}^{3}\eta_i^2 \right], \tag{6}$$

with dimensional constant Δf, numerical parameter α, ϵ_{ij} and b. Comparing with previous model [25], the last term $\prod_{i=1}^{3}\eta_i^2$ with a large coefficient b is added to remove the

undesired disturbance to a binary interface described in ref [31] and to keep the size of the contact triple point/line small. Since the grain growth in Figure 1 setup is no longer driven by curvature, an explicit driving force term ΔT coupled with an interpolation function $h = -\eta_1^3(10 - 15\eta_1 + 6\eta_1^2)$ is required.

The time evolution of the order parameters and, therefore, the evolution of the two grains follows Allen–Cahn phase-field dynamics

$$-\frac{\partial \eta_i}{\partial t} = L_i \frac{\delta F}{\delta \eta_i}, \tag{7}$$

with time t and kinetic coefficient L_i. This equation above applies to η_1 and η_2 only, while η_3 is fixed since the coarsening of pinning particles is a slow process at the grain growth time scale. A dimensionless form of Equation (7) is

$$-\frac{\partial \eta_i}{\partial t} = \tilde{L}_i \left(\frac{\partial (f_0/\Delta f)}{\partial \eta_i} + \Delta \tilde{T} \frac{\partial h}{\partial \eta_i} - w^2 \xi_i \nabla^2 \eta_{\mathrm{i}} \right), \tag{8}$$

where $\tilde{t} = t/\tau$, $\tilde{L}_i = \Delta f \tau L_i$, $\Delta \tilde{T} = \Delta T/\Delta f$ with characteristic length scale $w = \sqrt{K/\Delta f}$ and time scale τ.

To study particle pinning with the PF model above, one needs to incorporate the correct surface energies, which can be expressed as an integral of local energy density across the interface

$$\gamma = \int_{-\infty}^{+\infty} \left[f_0(\eta_1, \eta_2, \eta_3) + \frac{1}{2} \sum_{i=1}^{2} \xi_i K (\nabla \eta_i)^2 \right] \mathrm{d}n, \tag{9}$$

where n is the coordinate along surface normal. Dimensionless surface energies are used in numerics which are related to Equation (9) by $\tilde{\gamma} = \gamma/(w\Delta f)$. In the case of coherent particle pinning, a second-phase precipitate initially forms a coherent interface with the hosting grain, and switches to an incoherent interface when another grain takes over. As the particle-grain interface changes from coherent to incoherent, there is a significant increase in surface energy owing to the structural change of the interface. Based on Equation (9), with η_1, η_2, η_3 corresponding to grain 1, grain 2 and the pinning particle, respectively, the GB energy and the two surface energies between the second-phase particle and two adjacent grains are related to five control parameters ξ_1, ξ_2, ϵ_{ij} and a constant factors α. To set up a correct surface energy, the control parameters for each interface are: (a) GB (γ_3): ξ_1, ξ_2, ϵ_{12}, (b) incoherent interface (γ_1): ξ_1, ϵ_{13}, (c) coherent interface (γ_2): ξ_2, ϵ_{23}. Here, γ_1 and γ_2 can be first specified independently, but γ_3 has to be calculated later by varying ϵ_{12} once ξ_1 and ξ_2 are fixed. In the present work, we use $\alpha = 0.1$, $\xi_1 = 0.5$, $\xi_2 = 0.1$, $\epsilon_{13} = 0.386$, $\epsilon_{23} = 0.0849$, $\epsilon_{12} = 0.1428$, which correspond to a typical surface energy for the incoherent interface $\gamma_1 = 0.75\ \mathrm{Jm}^{-2}$, the coherent interface $\gamma_2 = 0.15\ \mathrm{Jm}^{-2}$ and the GB $\gamma_3 = 0.75\ \mathrm{Jm}^{-2}$ [32].

Equation (8) is then solved in cylindrical coordinates, where the z axis follows the direction of grain-boundary motion with triple junction parameter $b = 50$. The central difference scheme is used with space discretization $\Delta x/w = 0.4$, and the forward Euler method is used for time integration. The maximum pinning force can be numerically evaluated using the distortion of the GB [25]

$$F_z = \Delta\tilde{T}^{\max} \int \hat{n} \cdot \hat{z} dA, \tag{10}$$

where $\hat{n}$ is the grain-boundary surface normal, dA is the surface element, $\hat{z}$ is the unit vector in the z direction and $\Delta\tilde{T}^{\max}$ is the maximum driving force for a pinned GB. From the order parameter field η_1, the surface normal is calculated by $\hat{n} = \nabla\eta_1/|\nabla\eta_1|$. To avoid ambiguity, we calculate the surface normal with only the two nearest grid points of the $\eta_1 = 0.5$ contour. The $F_z$integral is then evaluated using simple trapezoidal method. In all PF simulations, $\Delta\tilde{T}^{\max}$ is increased by a step size of 10^{-5}.

With the prescribed surface energies, the maximum pinning force from a coherent spherical particle is calculated using this PF model. As shown in Figure 2, the pinning force from our PF model is in very good agreement with theoretical predictions (Equation (1)) for various particle sizes.

PF simulations are then used to compare with our analytical expression for a coherent spheroidal particle (Equation (4)). As shown in Figure 3, our PF model reproduces the predicted pinning force for coherent spheroidal particles with aspect ratios ranging from 0.5 to 2.0.

By comparing with theoretical predictions for coherent pinning particles and various particle aspect ratios, the PF model we constructed in previous sections has demonstrated its potential as a quantitative approach to model particle-pinning phenomenon in grain growth. In a previous work by Harun et al. [12], the pinning force was quantitatively measured based on the change of total surface energy as the GB moves through the pinning particle. The pinning force as a function of GB position was also computed and compared with Hellman's prediction using the macroscopic curvature approximation [33]. However, that work did not demonstrate the linear dependence of pinning force with particle size and was limited to deal with simple incoherent particles with spherical shape only. We also want to point out that this work ignored an important elastic feature of coherent precipitate, namely the misfit strain, which most of the existing theories did not consider [2–4]. Since the particle pinning force is only related

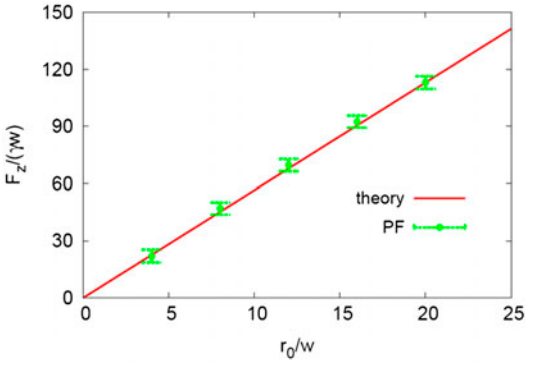

Figure 2. Comparison of the PF pinning force with theoretical prediction for various particle radius r_0. The theoretical line is given by Equation (1). The error in the PF results is evaluated based on the numerical integration in Equation (10).

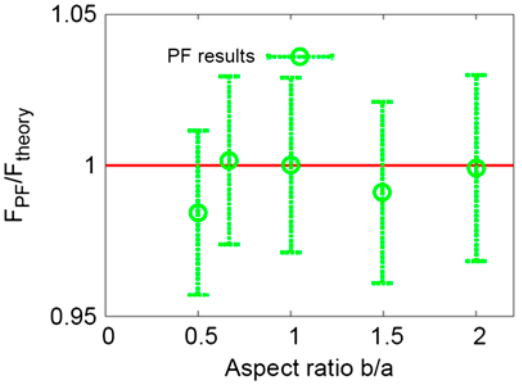

Figure 3. Pinning force from coherent spheroid particle. Here, we use particle size $a/w = 20$. The error in the PF results is evaluated based on the numerical integration in Equation (10).

to the triple-junction contact angle and the GB energy, and the effect of elastic energy on the triple-junction contact angle can be safely ignored as pointed out by Srolovitz et al. [36], the PF results we demonstrate in this work should be reasonable, especially for small misfit coherent particles.

With the proposed PF model, another important aspect of the particle-pinning phenomenon is examined, namely the grain boundary migration velocity. As demonstrated in the FEM method [13,16], the GB moves toward the pinning particle with an accelerated velocity during its initial approach to the particle, and then slows down as the GB passes the particle. If the grain growth driving force is large, the GB will eventually detach from the pinning particle and recover its migration velocity without pinning particles. In the case of a small driving force, the GB migration velocity will drop to zero, forming a stable GB-particle configuration. To our knowledge, all the results for GB migration velocity are based on incoherent pinning particles. With the proposed PF model, the GB migration velocity for coherent particles can be studied. Instead of using simple axi-symmetric cylindrical coordinates, the model (Equation (8)) is solved in full 3D here. The GB migration velocity is then evaluated using the formula $\mathrm{v} = \frac{1}{S}\int_s v_z ds$ proposed in a previous FEM study [16], where the average is over the whole boundary area S and z is the direction of GB motion.

In Figure 4, the GB migration velocity under the same driving force for both incoherent and coherent pinning particles are shown. The GB velocity for incoherent pinning particle shows the same features as the previous FEM results, but the velocity curve for coherent pinning particle is rather different. Under the same driving force, the moving GB can swipe through an incoherent pinning particle, but is completely pinned by a coherent particle of the same size. Instead of the initial attractive interaction between GB and pinning particle in the incoherent case, a coherent pinning particle demonstrates a restraining force from the beginning of GB-particle interaction. Inspection of simulation frames shows an unexpected GB behaviour. Rather than curving toward the particle at the beginning of the GB-particle interaction as found for incoherent particles (Figure 4, inlet I), the near particle boundary curves around the coherent particle without forming triple junctions even after the GB reache the pinning particle

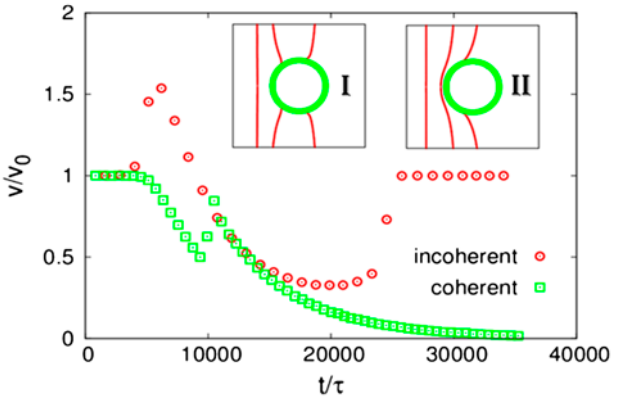

Figure 4. Grain boundary migration velocity as the GB approaches the pinning particle. Velocity is normalized by the GB velocity without pinning particles (v_0). Particle radius $r_0/w = 12$. Driving force $\Delta\tilde{T} = 0.0007$. The inlet I shows three GB positions (red line) in incoherent particle (green circle) pinning. Three GB lines correspond to bulk migration, initital attractive interaction and particle pinning configuration from left to right. The inlet II shows three GB positions (red line) in the coherent particle pinning. Three GB lines correspond to bulk migration, initital blocking interaction and particle pinning configuration from left to right.

(Figure 4, inlet II). Once the GB curvature reaches a critical value, triple junctions appear, and a fast moving spike is produced by quickly eliminating the curved GB around the particle. The disappearing of pulling behaviour in coherent particle pinning can be qualitatively understood by considering the relation $\cos\beta = (\gamma_1 - \gamma_2)/\gamma_3$. Since the surface energies follow $\gamma_2/\gamma_1 \ll 1$ and $\gamma_3/\gamma_1 \sim 1$ in this case, the angle β is always around 0; and therefore, the only possible configuration for GB is to wrap around the pinning particle (hence producing a blocking force for further migration) such that $\beta \rightarrow 0$ can be satisfied.

The pulling effect from a second-phase particle in front of a moving GB has been considered by Louat [34,35] and reviewed by Nes et al. [3] and by Manohar et al. [5] as an important improvement to Zener's original formula.With the demonstrated all-range blocking behaviour from coherent pinning particles, a modified Louat theory, which considers a restraining force instead of a pulling force, may be formulated.

To summarize this work, an analytical expression for the pinning force from a coherent spheroidal particle was derived and quantitatively validated using a phase-field model. By introducing a triple-phase term to previous PF particle pinning models, the large surface energy difference rising from the structural change of particle-grain interface was accurately incorporated in the model. The grain boundary migration velocity in the presence of coherent pinning particles demonstrated a restraining force over the whole GB-particle interaction range, which is qualitatively different from the case of incoherent pinning particles. The PF model for coherent particle pinning proposed in this work can be generalized in the context of multi-order parameter grain growth and could lead to a better understanding of coherent particle pinning phenomenon in polycrystalline materials.

Since this model is able to cover the large surface energy difference between coherent and incoherent surfaces, a semi-coherent interface which has a surface energy

between the two mentioned above could be easily included in this model. In a commonly seen case where the microstructure is pinned by more than one type of precipitates, the combined effect of coherent, incoherent and semi-coherent pinning particles is another interesting topic that can be simulated using the PF model proposed in this work.

Disclaimer

Acknowledgments

The authors would like to acknowledge the Strategic Center for Coal, NETL, for supporting this activity through the Innovative Process Technologies Program, and in particular Robert Romanosky as technology manager, Patricia Rawls as project manager and David Alman as ORD technical team coordinator.

References

[1] C.S. Smith, Trans. Metall. Soc. A.I.M.E. 175 (1948) p.15.
[2] M.F. Ashby, J. Harper and J. Lewis, Trans. Metall. Soc. A.I.M.E. 245 (1969) p.413.
[3] E. Nes, N. Ryum and O. Hunderi, Acta Metall. 33 (1985) p.11.
[4] W. Li and K.E. Easterling, Acta Metall. 38 (1990) p.1045.
[5] P.A. Manohar, M. Ferry and T. Chandra, ISIJ Intel. 38 (1998) p.913.
[6] D.J. Srolovitz, M.P. Anderson, G.S. Grest and P.S. Sahni, Acta Metall. 32 (1984) p.1429.
[7] R.D. Doherty, D.J. Srolovitz, A.D. Rollett and M.P. Anderson, Scripta Met. 21 (1987) p.675.
[8] J. Gao, R.G. Thompson and B.R. Patterson, Acta Mater. 45 (1997) p.3653.
[9] B.K. Kad and P.M. Hazzledine, Mater. Sci. Eng. A 238 (1997) p.70.
[10] M.A. Miodownik, J.W. Martin and A. Cerezo, Philos. Mag. 79 (1999) p.203.
[11] M. Miodownik, E.A. Holm and G.N. Hassold, Scripta Mater. 42 (2000) p.1173.
[12] A. Harun, E.A. Holm, M.P. Clode and M.A. Miodownik, Acta Mater. 54 (2006) p.3261.
[13] B.N. Kim and T. Kishi, Acta Mater. 47 (1999) p.2293.
[14] S.P. Riege, C.V. Thompson and H.J. Frost, Acta Mater. 47 (1999) p.1879.
[15] D. Weygand, Y. Bréchet and J. Lépinoux, Mater. Sci. Eng. A 292 (2000) p.34.
[16] G. Couturier, C. Maurice and R. Fortunier, Philos. Mag. 83 (2003) p.3387.
[17] G. Couturier, R. Doherty, C. Maurice and R. Fortunier, Acta Mater. 53 (2005) p.977.
[18] D. Fan, L. Chen and S.P. Chen, J. Am. Ceram. Soc. 81 (1998) p.526.
[19] N. Moelans, B. Blanpain and P. Wollants, Acta Mater. 54 (2006) p.1175.

[20] N. Moelans, B. Blanpain and P. Wollants, Acta Mater. 55 (2007) p.2173.
[21] Y. Suwa, Y. Saito and H. Onodera, Scripta Mater. 55 (2006) p.407.
[22] M. Apel, B. Böttger, J. Rudnizki, P. Schaffnit and I. Steinbach, ISIJ Int. 49 (2009) p.1024.
[23] L. Vanherpe, N. Moelans, B. Blanpain and S. Vandewalle, Comp. Mat. Sci. 49 (2010) p.340.
[24] Y. Suwa, Y. Saito and H. Onodera, Acta Mater. 55 (2007) p.6881.
[25] K. Chang and L. Chen, Modelling Simul. Mater. Sci. Eng. 20 (2012) p.055004.
[26] K. Chang, W. Feng and L. Chen, Acta Mater. 57 (2009) p.5229.
[27] N. Moelans, B. Blanpain and P. Wollants, Acta Mater. 53 (2005) p.1771.
[28] L.Q. Chen, Annu. Rev. Mater. Res. 32 (2002) p.113.
[29] W.J. Boettinger, J.A. Warren, C. Beckermann and A. Karma, Annu. Rev. Mater. Res. 32 (2002) p.163.
[30] L. Chen and W. Yang, Phys. Rev. B 50 (1994) p.15752.
[31] N. Moelans, B. Blanpain and P. Wollants, Phys. Rev. B 78 (2008) p.024113.
[32] J.M. Howe, *Interfaces in Materials*, 1997, p.378.
[33] P. Hellman and M. Hillert, Scand. J. Metall. 4 (1975) p.211.
[34] N. Louat, Acta Metall. 30 (1982) p.1291.
[35] N. Louat, Phil. Mag. 47 (1983) p.903.
[36] D.J. Srolovitz and S.H. Davis, Acta Mater. 49 (2001) p.1005.